Statistical Space-Time-Frequency Characterization of MIMO Shallow Water Acoustic Channels

Alenka G. Zajić
Naval Research Laboratory, Washington, DC 20375 USA

***Abstract*— This paper proposes a geometry-based statistical model for multiple-input multiple-output shallow water acoustic multipath fading channels. From the reference model, the corresponding space-time-frequency correlation function is derived. Finally, the derived spatial and temporal correlations are compared with the empirically obtained channel statistics and close agreement is observed[1].**

I. Introduction

Shallow water acoustic (SWA) communications find applications in oceanographic data collection, tactical surveillance, and offshore exploration. To make these applications feasible, there is a need for wireless underwater acoustic communications among deployed sensors and autonomous underwater vehicles. Statistical characterization of acoustic communication channels is necessary in order to assess system performance and improve the quality of a system [1].

The SWA channel is one of the most challenging communication channels because it suffers path-dependent Doppler and angle spreading, which results in a time-varying wideband channel impulse response with long delay spreads [2]. While several deterministic and statistical simulation models of SWA channel have been proposed [3]-[6], a statistical framework for SWA channels is still an open problem. In particular, the space-time-frequency correlation function is a necessary tool for a proper design and analysis of multiple-input multiple-output (MIMO) SWA communication systems. By taking into account only macro-scattering effects, Abdi and Guo [7] were the first to derive the space-frequency correlation function for *time-invariant* isovelocity SWA channels.

In contrast, this paper models a *time-varying* SWA channel by taking into account both macro- and micro-scattering effects. We first introduce a new geometry-based reference model for wideband MIMO SWA multipath fading channels. The proposed model characterizes the sound propagation in shallow water isovelocity environments by combining the deterministic ray-tracing theory with statistical methods needed to characterize random components of the propagation medium. From the reference model, the closed-form space-time-frequency correlation function (stf-cf) for a shallow water isovelocity environment is derived. The closed-form stf-cf can be useful for estimation of physical parameters of the channel, such as angle spread, mean angles of departure and arrival, etc. This allows system engineers to understand how these channel parameters affect the correlation, which in turn provides useful guidelines for the system design. To illustrate the utility of the proposed model, we compare the temporal and spatial correlation functions with those obtained from the measurements reported in [8], [9].

[1]This work has been supported by ONR.

The remainder of the paper is organized as follows. Section II introduces the geometry-based statistical model for wideband MIMO SWA multipath fading channels. Section III derives the stf-cf for a shallow water isovelocity environment. Section IV compares the analytical and empirical results for the temporal and spatial correlations. Finally, Section V provides some concluding remarks.

II. Geometry-based Statistical Model for Wideband MIMO SWA Channels

This paper considers a MIMO communication system with L_t transmit and L_r receive transducers. The propagation occurs in shallow water environments with a constant sound speed and is characterized by two-dimensional (2-D) wide sense stationary uncorrelated scattering (WSSUS) with either line-of-sight or non-line-of-sight conditions between the transmitter ($\mathrm{T_x}$) and receiver ($\mathrm{R_x}$). The MIMO SWA channel can be described by an $L_r \times L_t$ matrix $\mathbf{H}(t,\tau) = [h_{ij}(t,\tau)]_{L_r \times L_t}$ of the input-delay spread functions.

Fig. 1 shows a SWA channel with $L_t = L_r = 2$ transducer elements. This elementary 2×2 transducer configuration will be used later to construct uniform linear arrays with an arbitrary number of transducer elements. The SWA channel is modeled as a 2-D waveguide bounded from the top and bottom. The surface and bottom boundaries reflect an acoustic signal, which results in multiple eigenrays travelling between the $\mathrm{T_x}$ and $\mathrm{R_x}$, as shown in Fig. 1. The roughness of sea surface and sea bottom is characterized by S and B macro-scatterers, respectively. At any time instance t, the $\mathrm{R_x}$ receives $2S$ downward arriving eigenrays, each one having different number of s surface and b bottom reflections, where $1 \leq s \leq S$, and $s-1 \leq b \leq s$. Similarly, there are $2B$ upward arriving eigenrays with b bottom and s surface reflections, where $1 \leq b \leq B$ and $b-1 \leq s \leq b$. Note that exact positions of scatterers depend on the surface and bottom characteristics and may vary from one location to another and from one time instance to another. On the other hand, the average of scattering positions over different locations (or time instances) depends only on the waveguide geometry and the number of eigenrays, and can be computed. To implement this idea, each eigenray is modeled as an average of rays scattered from N_{sb} possible positions of surface scatterers and M_{bs} possible positions of bottom

Report Documentation Page

Form Approved
OMB No. 0704-0188

1. REPORT DATE	2. REPORT TYPE	3. DATES COVERED
JUN 2010	**N/A**	**-**

4. TITLE AND SUBTITLE	5a. CONTRACT NUMBER
Statistical Space-Time-Frequency Characterization of MIMO Shallow Water Acoustic Channels	5b. GRANT NUMBER
	5c. PROGRAM ELEMENT NUMBER
6. AUTHOR(S)	5d. PROJECT NUMBER
	5e. TASK NUMBER
	5f. WORK UNIT NUMBER
7. PERFORMING ORGANIZATION NAME(S) AND ADDRESS(ES) **Naval Research Laboratory, Washington, DC 20375 USA**	8. PERFORMING ORGANIZATION REPORT NUMBER
9. SPONSORING/MONITORING AGENCY NAME(S) AND ADDRESS(ES)	10. SPONSOR/MONITOR'S ACRONYM(S)
	11. SPONSOR/MONITOR'S REPORT NUMBER(S)

12. DISTRIBUTION/AVAILABILITY STATEMENT
Approved for public release, distribution unlimited

13. SUPPLEMENTARY NOTES
See also ADM202806. Proceedings of the Oceans 2009 MTS/IEEE Conference held in Biloxi, Mississippi on 26-29 October 2009. U.S. Government or Federal Purpose Rights License., The original document contains color images.

14. ABSTRACT
This paper proposes a geometry-based statistical model for multiple-input multiple-output shallow water acoustic multipath fading channels. From the reference model, the corresponding space-time-frequency correlation function is derived. Finally, the derived spatial and temporal correlations are compared with the empirically obtained channel statistics and close agreement is observed1.

15. SUBJECT TERMS

16. SECURITY CLASSIFICATION OF:			17. LIMITATION OF ABSTRACT	18. NUMBER OF PAGES	19a. NAME OF RESPONSIBLE PERSON
a. REPORT	b. ABSTRACT	c. THIS PAGE			
unclassified	**unclassified**	**unclassified**	**SAR**	**6**	

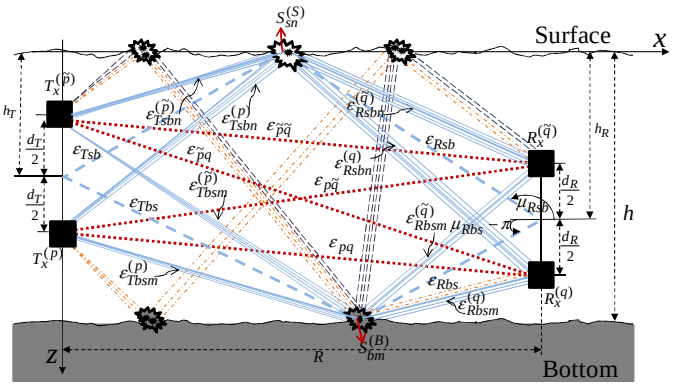

Fig. 1. The geometry-based model for a MIMO wideband SWA channel with $L_t = L_r = 2$ transducer elements.

scatterers (i.e., micro-scatterers), where the possible positions of scatterers are clustered around the averaged positions of scatterers, as shown in Fig. 1. The horizontal spacing between the $\mathrm{T_x}$ and $\mathrm{R_x}$ is denoted by R. The water depth is denoted by h, while the depths of $\mathrm{T_x}$ and $\mathrm{R_x}$ are denoted by h_T and h_R, respectively. As we are interested in medium and long range shallow water communications, we assume that the depths h, h_T, and h_R are much smaller than the distance R. The spacing between two adjacent transducer elements at the $\mathrm{T_x}$ and $\mathrm{R_x}$ is d_T and d_R, respectively. It is assumed that d_T and d_R are much smaller than the depths h, h_T, and h_R. The symbols $\epsilon^{(p)}_{Tsbn}$ and $\epsilon^{(p)}_{Tbsm}$ denote distances $T^{(p)}_x$-$S^{(S)}_{sn}$ and $T^{(p)}_x$-$S^{(B)}_{bm}$, respectively, where $S^{(S)}_{sn}$ and $S^{(B)}_{bm}$ denote the n^{th} and m^{th} micro-scatterers at the surface and bottom, respectively, for $1 \le n \le N_{tb}$ and $1 \le m \le M_{bt}$, as shown in Fig. 1. Similarly, the symbols $\epsilon^{(\tilde{p})}_{Tsbn}$, $\epsilon^{(\tilde{p})}_{Tbsm}$, $\epsilon^{(q)}_{Rsbn}$, $\epsilon^{(q)}_{Rbsm}$, $\epsilon^{(\tilde{q})}_{Rsbn}$, $\epsilon^{(\tilde{q})}_{Rbsm}$, ϵ_{pq}, $\epsilon_{\tilde{p}q}$, $\epsilon_{p\tilde{q}}$, and $\epsilon_{\tilde{p}\tilde{q}}$ denote distances $T^{(\tilde{p})}_x$-$S^{(S)}_{sn}$, $T^{(\tilde{p})}_x$-$S^{(B)}_{bm}$, $S^{(S)}_{sn}$-$R^{(q)}_x$, $S^{(B)}_{bm}$-$R^{(q)}_x$, $S^{(S)}_{sn}$-$R^{(\tilde{q})}_x$, $S^{(B)}_{bm}$-$R^{(\tilde{q})}_x$, $T^{(p)}_x$-$R^{(q)}_x$, $T^{(\tilde{p})}_x$-$R^{(q)}_x$, $T^{(p)}_x$-$R^{(\tilde{q})}_x$, and $T^{(\tilde{p})}_x$-$R^{(\tilde{q})}_x$, respectively. For ease

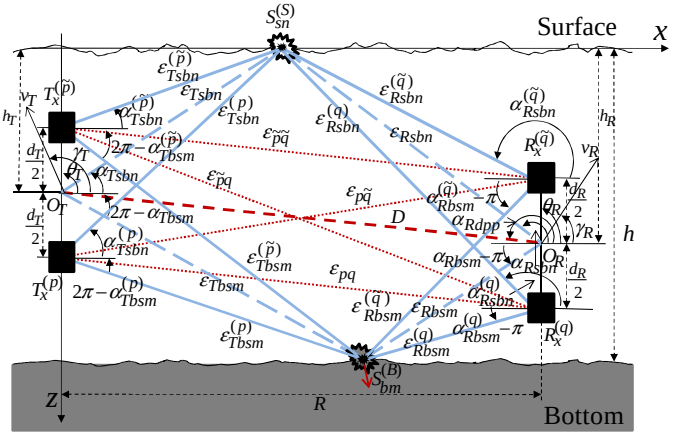

Fig. 2. The detailed geometry of the DPP, single-bounced surface, and single-bounced bottom eigenrays scattered from the n^{th} and m^{th} micro-scatterer, respectively.

of reference, Fig. 2 details the geometry of the deterministic (direct) propagation paths (DPP) as well as the geometry of single-bounced surface and single-bounced bottom eigenrays (i.e., $s = 1, b = 0$, $s = 0, b = 1$) scattered from the n^{th} and m^{th} micro-scatterers, respectively. Angles θ_T and θ_R in Fig. 2 describe the orientations of $\mathrm{T_x}$ and $\mathrm{R_x}$ transducer arrays in the x-z plane, respectively, relative to the x-axis. The $\mathrm{T_x}$ and $\mathrm{R_x}$ are moving with speeds v_T and v_R in directions described by angles γ_T and γ_R in the x-z plane (relative to the x-axis), respectively. The symbols $\alpha^{(p)}_{Tsbn}$ and $\alpha^{(p)}_{Tbsm}$ are the angles of departure (AoD) of eigenrays that start from $T^{(p)}_x$ and impinge on the scatterers $S^{(S)}_{sn}$ and $S^{(B)}_{bm}$, respectively, whereas $\alpha^{(q)}_{Rsbn}$ and $\alpha^{(q)}_{Rbsm}$ are the angles of arrival (AoA) of the eigenrays scattered from $S^{(S)}_{tn}$ and $S^{(B)}_{bm}$ and arriving at $R^{(q)}_x$, respectively. Finally, the symbols α_{Rdpp} and D denote the AoA of DPP ray and the distance O_T-O_R, respectively.

Observe from the geometrical model in Fig. 1 that propagation through SWA channel can be characterized as a superposition of surface-bottom bounced eigenrays and the DPP eigenray between the $\mathrm{T_x}$ and $\mathrm{R_x}$. The multiple bounced rays can be grouped into the upward arriving (UA) rays (i.e., the last reflection is from the bottom) and the downward arriving (DA) rays (i.e., the last reflection is from the surface). Then, the input delay-spread function of the pressure link $T^{(p)}_x$-$R^{(q)}_x$ can be written as a superposition of the DPP, UA, and DA rays, viz.

$$h_{pq}(t,\tau) \;=\; h^{DPP}_{pq}(t,\tau) + h^{UA}_{pq}(t,\tau) + h^{DA}_{pq}(t,\tau). \quad (1)$$

The DPP component of the input delay-spread function is

$$h^{DPP}_{pq}(t,\tau) \;=\; \sqrt{\frac{K}{K+1}}\sqrt{G_p\left(\alpha_{Rddp}+\pi\right)G_q\left(\alpha_{Rdpp}\right)} \times\; L_S(D)L_A(D)\delta\left(\tau-\tau^{(p,q)}_{dpp}(t)\right), \quad (2)$$

where $G_p(\cdot)$ and $G_q(\cdot)$ denote the radiation patterns of the p^{th} transmit and q^{th} receive transducer element, respectively, K is the Rice factor (ratio of DPP to scatter received power), $L_S(D)$ and $L_A(D)$ denote the propagation loss due to spherical spreading and absorption, respectively, and $\delta(\cdot)$ denotes the Dirac impulse function. The DPP time delay $\tau^{(p,q)}_{dpp}(t)$ denotes the travel time of the direct ray between $T^{(p)}_x$ and $R^{(q)}_x$, i.e.,

$$\tau^{(p,q)}_{dpp}(t) \;=\; \frac{\epsilon_{pq}}{c} + \frac{v_T}{c}t\cos(\alpha_{Rdpp}+\pi-\gamma_T) + \frac{v_R}{c}t\cos(\alpha_{Rdpp}-\gamma_R), \quad (3)$$

where c is the speed of sound. We assume that the $\mathrm{T_x}$ has omnidirectional transducer elements and therefore produces a spherical wavefront in an isovelocity medium. The propagation loss caused by the spherical spreading can be written as [10] $L_S(D) = 1/D$. Furthermore, when sound propagates in the ocean, part of the acoustic energy is continuously transformed into heat. This absorption is primarily a result of relaxation processes in seawater. The absorption loss can be written as [10]

$$L_A(D) = 10^{-D\beta/20000}, \quad (4)$$

where

$$\beta = 8.68 \cdot 10^3 \times \left(\frac{S \cdot A \cdot f_T \cdot f_c^2}{f_T^2 + f_c^2} + \frac{B \cdot f^2}{f_T}(1 - 6.54 \cdot 10^{-4} \cdot P)\right) \text{ [dB/km]}, \quad (5)$$

where $A = 2.34 \cdot 10^{-6}$, $B = 3.38 \cdot 10^{-6}$, S is salinity (in ‰), P is hydrostatic pressure [kg/cm^2], f_c is the carrier frequency [kHz] and $f_T = 21.9 \cdot 10^{6-1520/(T+273)}$ is relaxation frequency [kHz], with T as the temperature [$^\circ C$].

The upward and downward arriving components of the input delay-spread function are, respectively,

$$h_{pq}^{UA}(t,\tau) = \sqrt{\frac{\eta_B}{2B(K+1)}} \sum_{b=1}^{B} \sum_{s=b-1}^{b} L_S(D_{bs}) L_A(D_{bs}) \times L_B(\theta_{bs})^b \sqrt{\frac{1}{M_{bs}}} \sum_{m=1}^{M_{bs}} \sqrt{G_p\left(\alpha_{Tbsm}^{(p)}\right) G_q\left(\alpha_{Rbsm}^{(q)}\right)} \times \xi_{bsm} e^{j\phi_{bsm}} \delta\left(\tau - \tau_{bsm}^{(p,q)}(t)\right), \quad (6)$$

$$h_{pq}^{DA}(t,\tau) = \sqrt{\frac{\eta_S}{2S(K+1)}} \sum_{s=1}^{S} \sum_{b=s-1}^{s} L_S(D_{sb}) L_A(D_{sb}) \times L_B(\theta_{sb})^b \sqrt{\frac{1}{N_{sb}}} \sum_{n=1}^{N_{sb}} \sqrt{G_p\left(\alpha_{Tsbn}^{(p)}\right) G_q\left(\alpha_{Rsbn}^{(q)}\right)} \times \xi_{sbn} e^{j\phi_{sbn}} \delta\left(\tau - \tau_{sbn}^{(p,q)}(t)\right), \quad (7)$$

where $\xi_{bsm} > 0$ and $\xi_{sbn} > 0$ denote the amplitudes, ϕ_{sbn} and ϕ_{bsm} denote the phases of multipath components, $L_S(D_{sb})$ and $L_S(D_{bs})$ denote the propagation loss due to spherical spreading, and $L_A(D_{sb})$ and $L_A(D_{bs})$ denote the propagation loss due to absorption, where D_{sb} and D_{bs} denote the total distances travelled by UA and DA rays with s surface and b bottom reflections. These distances are obtained using the method of images and can be written as [10]

$$D_{sb} = \sqrt{R^2 + (2bh + h_R - (-1)^{(s-b)} h_T)^2}, \quad (8)$$

$$D_{bs} = \sqrt{R^2 + (2sh - h_R + (-1)^{(b-s)} h_T)^2}. \quad (9)$$

The parameters η_S and η_B in (6) and (7), respectively, specify how much the UA and DA rays contribute in the total power, i.e., these parameters satisfy $\eta_S + \eta_B = 1$. The parameters $L_B(\theta_{sb})$ and $L_B(\theta_{bs})$ denote the impedance mismatch between the seawater and seabed and can be written as [10]

$$L_B(\theta) = \left| \frac{m\cos\theta - \sqrt{n^2 - \sin^2\theta}}{m\cos\theta + \sqrt{n^2 - \sin^2\theta}} \right|, \quad (10)$$

where $m = \rho_1/\rho$, $n = c/c1$, ρ and c denote the density and sound speed in the seawater, respectively, whereas ρ_1 and c_1 denote the density and sound speed in the seabed, respectively. The incidence angles θ_{sb} and θ_{bs} are obtained as follows:

$$\theta_{sb} = \tan^{-1}\left(\frac{R}{2bh + h_R - (-1)^{(s-b)} h_T}\right), \quad (11)$$

$$\theta_{bs} = \tan^{-1}\left(\frac{R}{2sh - h_R + (-1)^{(b-s)} h_T}\right). \quad (12)$$

Finally, the time delays $\tau_{bsm}^{(p,q)}(t)$ and $\tau_{sbn}^{(p,q)}(t)$ are the travel times of UA and DA rays with s surface and b bottom reflections, respectively, i.e.,

$$\tau_{sbn}^{(p,q)}(t) = \frac{D_{sb}}{c} - \frac{\epsilon_{Tsb} - \epsilon_{Tsbn}^{(p)}}{c} - \frac{\epsilon_{Rsb} - \epsilon_{Rsbn}^{(q)}}{c} + \frac{1}{c}\Delta Z_{sbn}(t)\sin\alpha_{Rsbn}^{(q)} + \frac{1}{c}\left[v_T t\cos(\alpha_{Tsbn}^{(p)} - \gamma_T) + v_R t\cos(\alpha_{Rsbn}^{(q)} - \gamma_R)\right], \quad (13)$$

$$\tau_{bsm}^{(p,q)}(t) = \frac{D_{bs}}{c} - \frac{\epsilon_{Tbs} - \epsilon_{Tbsm}^{(p)}}{c} - \frac{\epsilon_{Rbs} - \epsilon_{Rbsm}^{(q)}}{c} + \frac{1}{c}\Delta Z_{bsm}(t)\sin\alpha_{Rbsm}^{(q)} + \frac{1}{c}\left[v_T t\cos(\alpha_{Tbsm}^{(p)} - \gamma_T) + v_R t\cos(\alpha_{Rbsm}^{(q)} - \gamma_R)\right], \quad (14)$$

where $\Delta Z_{sbn}(t)$ and $\Delta Z_{bsm}(t)$ denote the vertical displacements of surface scatterers due to the surface motion and the distances ϵ_{Tsb}, ϵ_{Rsb}, ϵ_{Tbs}, and ϵ_{Rbs} are defined in Fig. 1.

It is assumed that the AoDs ($\alpha_{Tsbn}^{(p)}$ and $\alpha_{Tbsm}^{(p)}$), the AoAs ($\alpha_{Rsbn}^{(q)}$ and $\alpha_{Rbsm}^{(q)}$), and the vertical displacements $\Delta Z_{sbn}(t)$ and $\Delta Z_{bsm}(t)$ are random variables. Furthermore, it is assumed that the phases ϕ_{sbn} and ϕ_{bsm} are uniform random variables on the interval $[-\pi, \pi)$ that are independent from the AoDs, the AoAs, and the vertical displacements at the surface. Note that the AoDs ($\alpha_{Tsbn}^{(p)}$ and $\alpha_{Tbsm}^{(p)}$) are dependent on the AoAs ($\alpha_{Rsbn}^{(q)}$ and $\alpha_{Rbsm}^{(q)}$), respectively. Assuming small angle spreads, $d_T \ll \min(h_T, h - h_T)$, and $d_R \ll \min(h_R, h - h_R)$, we can approximate the DoAs and AoAs in Fig. 2 as $\alpha_{Tsbn}^{(p)} \approx \alpha_{Tsbn}^{(\tilde{p})} \approx \alpha_{Tsbn}$, $\alpha_{Tbsm}^{(p)} \approx \alpha_{Tbsm}^{(\tilde{p})} \approx \alpha_{Tbsm}$, $\alpha_{Rsbn}^{(q)} \approx \alpha_{Rsbn}^{(\tilde{q})} \approx \alpha_{Rsbn}$, and $\alpha_{Rbsm}^{(q)} \approx \alpha_{Rbsm}^{(\tilde{q})} \approx \alpha_{Rbsm}$, where α_{Tsbn}, α_{Tbsm}, α_{Rsbn}, and α_{Rbsm} are shown in Fig. 2. Assuming that each ray, when interacting with the surface and bottom, has equal incident and reflecting angles, we can observe that $\alpha_{Tsbn} = \pi - \alpha_{Rsbn}$ and $\alpha_{Tbsm} = 3\pi - \alpha_{Rbsm}$.

The distances $\epsilon_{Tsbn}^{(p)}$, $\epsilon_{Tbsm}^{(p)}$, $\epsilon_{Rsbn}^{(q)}$, $\epsilon_{Rbsm}^{(q)}$, and ϵ_{pq} can be expressed as functions of the random angles α_{Rsbn} and α_{Rbsm} and the angle α_{Rdpp} as follows

$$\epsilon_{Tsbn}^{(p)} \approx \frac{h_T}{\sin\alpha_{Rsbn}} + \frac{L_t + 1 - 2p}{2} d_T\cos(\alpha_{Rsbn} + \theta_T) \quad (15)$$

$$\epsilon_{Tbsm}^{(p)} \approx -\frac{h - h_T}{\sin\alpha_{Rbsm}} + \frac{L_t + 1 - 2p}{2} d_T\cos(\alpha_{Rbsm} + \theta_T) \quad (16)$$

$$\epsilon_{Rsbn}^{(q)} \approx \frac{h_R}{\sin\alpha_{Rsbn}} - \frac{L_r + 1 - 2q}{2} d_R\cos(\alpha_{Rsbn} - \theta_R) \quad (17)$$

$$\epsilon_{Rbsm}^{(q)} \approx -\frac{h - h_R}{\sin\alpha_{Rbsm}} - \frac{L_r + 1 - 2q}{2} d_R\cos(\alpha_{Rbsm} - \theta_R) \quad (18)$$

$$\epsilon_{pq} \approx \sqrt{R^2 + (h_T - h_R)^2} + \frac{L_t + 1 - 2p}{2} d_T\cos(\alpha_{Rdpp} - \theta_T) - \frac{L_r + 1 - 2q}{2} d_R\cos(\alpha_{Rdpp} - \theta_R), \quad (19)$$

where parameters p and q take values from the sets $p \in \{1, \ldots, L_t\}$ and $q \in \{1, \ldots, L_r\}$, respectively. The derivations of approximations in (15)-(19) are omitted for brevity. To simplify further analysis, we normalize all time delays with respect to the direct arrival time. This normalization is reflected in the distances ϵ_{pq}, D_{sb}, and D_{bs}. Furthermore,

since the depths h, h_T, and h_R are much smaller than the distance R, the distances D_{sb} and D_{bs} can be approximated using $\sqrt{1+x} \approx 1 + x/2$, for small x. Hence, the distances ϵ_{pq}, D_{sb}, and D_{bs} can be approximated as

$$\epsilon_{pq} \approx 0.5(L_t + 1 - 2p)d_T \cos(\alpha_{Rdpp} - \theta_T) - 0.5(L_r + 1 - 2q)d_R \cos(\alpha_{Rdpp} - \theta_R), \quad (20)$$

$$D_{sb} \approx \frac{2}{R}[b^2h^2 + bhh_R - (-1)^{(s-b)}bhh_T + (s-b)h_Th_R], \quad (21)$$

$$D_{bs} \approx \frac{2}{R}[s^2h^2 - shh_R + (-1)^{(b-s)}shh_T + (b-s)h_Th_R]. \quad (22)$$

Finally, we note that ϵ_{Tsb}, ϵ_{Rsb}, ϵ_{Tbs}, and ϵ_{Rbs} can be written as functions of the mean AoA angles μ_{Rsb} and μ_{Rbs}, i.e., $\epsilon_{Tsb} = h_T/\sin\mu_{Rsb}$, $\epsilon_{Rsb} = h_R/\sin\mu_{Rsb}$, $\epsilon_{Tbs} = -(h - h_T)/\sin\mu_{Rbs}$, and $\epsilon_{Rbs} = -(h - h_R)/\sin\mu_{Rbs}$, where the mean AoA angles μ_{Rsb} and μ_{Rbs} are depicted in Fig. 1.

The angles of arrival α_{Rsbn} and α_{Rbsm} are modeled using the following Gaussian probability density functions (pdfs)

$$f_{\text{top}}(\alpha_{Rsbn}) = \frac{1}{\sqrt{2\pi\sigma^2_{Rsb}}} \exp\left\{-\frac{(\alpha_{Rsbn} - \mu_{Rsb})^2}{(2\sigma^2_{Rsb})}\right\}, \quad \text{for} \quad 0 < \alpha_{Rsbn} < \pi, \quad (23)$$

$$f_{\text{bottom}}(\alpha_{Rbsm}) = \frac{1}{\sqrt{2\pi\sigma^2_{Rbs}}} \exp\left\{-\frac{(\alpha_{Rbsm} - \mu_{Rbs})^2}{(2\sigma^2_{Rbs})}\right\}, \quad \text{for} \quad \pi < \alpha_{Rbsm} < 2\pi, \quad (24)$$

where μ_{Rsb} and μ_{Rbs} denote the the mean AoAs, whereas σ_{Rsb} and σ_{Rbs} denote the angle spreads.

Finally, the vertical displacements $\Delta Z_{sbn}(t)$ and $\Delta Z_{bsm}(t)$ are modeled as zero-mean Gaussian random processes with stationary and independent increments, i.e.,

$$f(\Delta Z_{sbn}(t)) = \frac{1}{\sqrt{2\pi t\zeta^2_{\Delta Z_{sb}}}} \exp\left\{-\frac{(\Delta Z_{sbn}(t))^2}{(2t\zeta^2_{\Delta Z_{sb}})}\right\}, \quad (25)$$

$$f(\Delta Z_{bsm}(t)) = \frac{1}{\sqrt{2\pi t\zeta^2_{\Delta Z_{bs}}}} \exp\left\{-\frac{(\Delta Z_{bsm}(t))^2}{(2t\zeta^2_{\Delta Z_{bs}})}\right\}, \quad (26)$$

where $t\zeta^2_{\Delta Z_{sb}}$ and $t\zeta^2_{\Delta Z_{bs}}$ denote variances.

To simplify further analysis, we use the time-variant transfer function instead of the input delay-spread function and we normalize the gain patterns of the transducer elements to unity (i.e., we assume omnidirectional array elements), although other gain patterns can be accommodated at this point. The time-variant transfer function is the Fourier transform of the input delay-spread function and can be written as

$$P_{pq}(t,f) = \mathcal{F}_\tau\{h_{pq}(t,\tau)\} = P^{DPP}_{pq}(t,f) + P^{UA}_{pq}(t,f) + P^{DA}_{pq}(t,f) \quad (27)$$

where $P^{DPP}_{pq}(t,f)$, $P^{UA}_{pq}(t,f)$, and $P^{DA}_{pq}(t,f)$ are DPP, UA, and DA components of the time-variant transfer function, respectively. Using (2)-(22), the DPP, UA, and DA components of the time-variant transfer function in (27) can be written as

$$P^{DPP}_{pq}(t,f) = \mathcal{F}_\tau\left\{h^{DPP}_{pq}(t,\tau)\right\} = \sqrt{\frac{K}{K+1}} L_S(D)L_A(D) \; e^{j\frac{2\pi f_c}{c}[v_T t\cos(\alpha_{Rdpp}-\gamma_T) - v_R t\cos(\alpha_{Rdpp}-\gamma_R)]} \; e^{j\frac{2\pi f_c}{c}(0.5L_t+0.5-p)d_T\cos(\alpha_{Rdpp}-\theta_T)} \; e^{-j\frac{2\pi f_c}{c}(0.5L_r+0.5-q)d_R\cos(\alpha_{Rdpp}-\theta_R)}, \quad (28)$$

$$P^{UA}_{pq}(t,f) = \mathcal{F}_\tau\left\{h^{UA}_{pq}(t,\tau)\right\} = \sqrt{\frac{\eta_B}{2B(K+1)}} \sum_{b=1}^{B}\sum_{s=b-1}^{b} L_S(D_{bs})L_A(D_{bs})L_B(\theta_{bs})^b \sqrt{\frac{1}{M_{bs}}}\sum_{m=1}^{M_{bs}} \xi_{bsm} e^{j\phi_{bsm}} \; e^{-j\frac{2\pi f}{c}\left[D_{bs} - \frac{h_R+h_T-2h}{\sin\mu_{Rbs}} + \frac{h_R+h_T-2h}{\sin\alpha_{Rbsm}}\right]} \; e^{j\frac{2\pi f_c}{c}[v_T t\cos(\alpha_{Rbsm}+\gamma_T) - v_R t\cos(\alpha_{Rbsm}-\gamma_R) - \Delta Z_{bsm}(t)\sin\alpha_{Rbsm}]} \; e^{j\frac{2\pi f_c}{c}[\frac{L_t+1-2p}{2}d_T\cos(\alpha_{Rbsm}+\theta_T) - \frac{L_r+1-2q}{2}d_R\cos(\alpha_{Rbsm}-\theta_R)]}, \quad (29)$$

$$P^{DA}_{pq}(t,f) = \mathcal{F}_\tau\left\{h^{DA}_{pq}(t,\tau)\right\} = \sqrt{\frac{\eta_T}{2T(K+1)}} \sum_{s=1}^{S}\sum_{b=s-1}^{s} L_S(D_{sb})L_A(D_{sb})L_B(\theta_{sb})^b \sqrt{\frac{1}{N_{sb}}}\sum_{n=1}^{N_{sb}} \xi_{sbn} e^{j\phi_{sbn}} \; e^{-j\frac{2\pi f}{c}\left[D_{sb} - \frac{h_R+h_T}{\sin\mu_{Rsb}} + \frac{h_R+h_T}{\sin\alpha_{Rsbn}}\right]} \; e^{j\frac{2\pi f_c}{c}[v_T t\cos(\alpha_{Rsbn}+\gamma_T) - v_R t\cos(\alpha_{Rsbn}-\gamma_R) - \Delta Z_{sbn}(t)\sin\alpha_{Rsbn}]} \; e^{j\frac{2\pi f_c}{c}[\frac{L_t+1-2p}{2}d_T\cos(\alpha_{Rsbn}+\theta_T) - \frac{L_r+1-2q}{2}d_R\cos(\alpha_{Rsbn}-\theta_R)]}. \quad (30)$$

III. Space-Time-Frequency Correlation Function of the Statistical Model

Assuming a 2-D WSSUS isovelocity shallow water environment, we here derive the stf-cf of the geometry-based statistical model. The normalized stf-cf between two time-variant transfer functions $P_{pq}(t,f)$ and $P_{\tilde{p}\tilde{q}}(t+\Delta t, f+\Delta f)$, is defined as

$$R_{pq,\tilde{p}\tilde{q}}(\Delta t, \Delta f) = \frac{\mathrm{E}\left[P_{pq}(t,f)^* P_{\tilde{p}\tilde{q}}(t+\Delta t, f+\Delta f)\right]}{\sqrt{\mathrm{E}[|P_{pq}(t,f)|^2]\mathrm{E}[|P_{\tilde{p}\tilde{q}}(t,f)|^2]}}, \quad (31)$$

where $(\,\cdot\,)^*$ denotes complex conjugate operation, $\mathrm{E}[\,\cdot\,]$ is the statistical expectation operator, $p, \tilde{p} \in \{1,\ldots,L_t\}$, and $q, \tilde{q} \in \{1,\ldots,L_r\}$. Since $P^{UA}_{pq}(t,f)$ and $P^{DA}_{pq}(t,f)$ are independent zero-mean random processes, (31) can be simplified to

$$R_{pq,\tilde{p}\tilde{q}}(\Delta t, \Delta f) = R^{DPP}_{pq,\tilde{p}\tilde{q}}(\Delta t, \Delta f) + R^{UA}_{pq,\tilde{p}\tilde{q}}(\Delta t, \Delta f) + R^{DA}_{pq,\tilde{p}\tilde{q}}(\Delta t, \Delta f), \quad (32)$$

where $R^{DPP}_{pq,\tilde{p}\tilde{q}}(\Delta t, \Delta f)$, $R^{UA}_{pq,\tilde{p}\tilde{q}}(\Delta t, \Delta f)$, and $R^{DA}_{pq,\tilde{p}\tilde{q}}(\Delta t, \Delta f)$ denote the normalized stf-cfs of the DPP, UA, and DA components, respectively, and are defined as

$$R^{DPP}_{pq,\tilde{p}\tilde{q}}(\Delta t, \Delta f) = \frac{\mathrm{E}\left[P^{DPP}_{pq}(t,f)^* P^{DPP}_{\tilde{p}\tilde{q}}(t+\Delta t, f+\Delta f)\right]}{\Omega_{DPP}/(K+1)} \quad (33)$$

$$R^{UA}_{pq,\tilde{p}\tilde{q}}(\Delta t, \Delta f) = \frac{\mathrm{E}\left[P^{UA}_{pq}(t,f)^* P^{UA}_{\tilde{p}\tilde{q}}(t+\Delta t, f+\Delta f)\right]}{\Omega_{UA}/(K+1)} \quad (34)$$

$$R^{DA}_{pq,\tilde{p}\tilde{q}}(\Delta t, \Delta f) = \frac{\mathrm{E}\left[P^{DA}_{pq}(t,f)^* P^{DA}_{\tilde{p}\tilde{q}}(t+\Delta t, f+\Delta f)\right]}{\Omega_{DA}/(K+1)} \quad (35)$$

where $\Omega_{UA} = \mathrm{E}[L_S(D_{bs})L_A(D_{bs})L_B(\theta_{bs})^b]$, $\Omega_{DPP} = L_S(D)L_A(D)$, and $\Omega_{DA} = \mathrm{E}[L_S(D_{sb})L_A(D_{sb})L_B(\theta_{sb})^b]$.

By substituting (28) into (33), the expression for the stf-cf of DPP component becomes

$$R^{DPP}_{pq,\tilde{p}\tilde{q}}(\Delta t,\Delta f) = K$$
$$e^{j\frac{2\pi f_c}{c}[v_T\Delta t\cos(\alpha_{Rdpp}-\gamma_T)-v_R\Delta t\cos(\alpha_{Rdpp}-\gamma_R)]}$$
$$e^{j\frac{2\pi f_c}{c}[(p-\tilde{p})d_T\cos(\alpha_{Rdpp}-\theta_T)-(q-\tilde{q})d_R\cos(\alpha_{Rdpp}-\theta_R)]}. \quad (36)$$

Substituting (29) and (30) into (34) and (35), respectively, noting that the phases ϕ_{bsm} and ϕ_{sbn} are independent and uniformly distributed over $[-\pi,\pi)$, and assuming that $M_{bs}\gg 1$ and $N_{sb}\gg 1$, the stf-cfs of the UA and DA components can be written as, respectively,

$$R^{UA}_{pq,\tilde{p}\tilde{q}}(\Delta t,\Delta f) = \frac{\eta_B}{2B}\sum_{b=1}^{B}\sum_{s=b-1}^{b}\int_{\pi}^{2\pi}\frac{1}{\sqrt{2\pi\sigma^2_{Rbs}}} \quad (37)$$
$$e^{-\frac{(\alpha_{Rbs}-\mu_{Rbs})^2}{2\sigma^2_{Rbs}}}e^{-j\frac{2\pi\Delta f}{c}\left[D_{bs}-\frac{h_R+h_T-2h}{\sin\mu_{Rbs}}+\frac{h_R+h_T-2h}{\sin\alpha_{Rbs}}\right]}$$
$$e^{j\frac{2\pi f_c}{c}[(p-\tilde{p})d_T\cos(\alpha_{Rbs}+\theta_T)-(q-\tilde{q})d_R\cos(\alpha_{Rbs}-\theta_R)]}$$
$$e^{j\frac{2\pi f_c}{c}[v_T\Delta t\cos(\alpha_{Rbs}+\gamma_T)-v_R\Delta t\cos(\alpha_{Rbs}-\gamma_R)]}$$
$$e^{-\frac{\Delta t\zeta^2_{\Delta Z_{bs}}}{2}[\frac{2\pi f_c}{c}\sin\alpha_{Rbs}]^2}d\alpha_{Rbs},$$
$$R^{DA}_{pq,\tilde{p}\tilde{q}}(\Delta t,\Delta f) = \frac{\eta_S}{2S}\sum_{s=1}^{S}\sum_{b=s-1}^{s}\int_{0}^{\pi}\frac{1}{\sqrt{2\pi\sigma^2_{Rsb}}} \quad (38)$$
$$e^{-\frac{(\alpha_{Rsb}-\mu_{Rsb})^2}{2\sigma^2_{Rsb}}}e^{-j\frac{2\pi\Delta f}{c}\left[D_{sb}-\frac{h_R+h_T}{\sin\mu_{Rsb}}+\frac{h_R+h_T}{\sin\alpha_{Rsb}}\right]}$$
$$e^{j\frac{2\pi f_c}{c}[(p-\tilde{p})d_T\cos(\alpha_{Rsb}+\theta_T)-(q-\tilde{q})d_R\cos(\alpha_{Rsb}-\theta_R)]}$$
$$e^{j\frac{2\pi f_c}{c}[v_T\Delta t\cos(\alpha_{Rsb}+\gamma_T)-v_R\Delta t\cos(\alpha_{Rsb}-\gamma_R)]}$$
$$e^{-\frac{\Delta t\zeta^2_{\Delta Z_{sb}}}{2}[\frac{2\pi f_c}{c}\sin\alpha_{Rsb}]^2}d\alpha_{Rsb}.$$

For small angle spreads, the AoAs α_{Rsb} and α_{Rbs} are mainly concentrated around the mean AoAs μ_{Rsb} and μ_{Rbs}, respectively. Using the first-order Taylor expansion, the AoA angles can be approximated as follows

$$\cos(\alpha_{Rsb}) \approx \cos(\mu_{Rsb}) - \sin(\mu_{Rsb})(\alpha_{Rsb}-\mu_{Rsb}), \quad (39)$$
$$\sin(\alpha_{Rsb}) \approx \sin(\mu_{Rsb}) + \cos(\mu_{Rsb})(\alpha_{Rsb}-\mu_{Rsb}), \quad (40)$$
$$\sin(\alpha_{Rsb})^2 \approx \sin(\mu_{Rsb})^2 + 2\sin(\mu_{Rsb})\cos(\mu_{Rsb})(\alpha_{Rsb}-\mu_{Rsb}), \quad (41)$$
$$\sin(\alpha_{Rsb})^{-1} \approx \sin(\mu_{Rsb})^{-1} - \cos(\mu_{Rsb})(\alpha_{Rsb}-\mu_{Rsb})/\sin(\mu_{Rsb})^{-2}. \quad (42)$$

The similar approximations are applied to the AoAs α_{Rbs}. Using these trigonometric approximations and the equality $\int e^{j\alpha x}(2\pi\sigma^2)^{-1/2}e^{-x^2/(2\sigma^2)}dx = e^{-\sigma^2\alpha^2/2}$ [7], the stf-cfs of UA and DA components can be closely approximated as

$$R^{UA}_{pq,\tilde{p}\tilde{q}}(\Delta t,\Delta f) = \frac{\eta_B}{2B}\sum_{b=1}^{B}\sum_{s=b-1}^{b}e^{-\frac{\Delta t\zeta^2_{\Delta Z_{bs}}}{2}[\frac{2\pi f_c}{c}\sin\mu_{Rbs}]^2} \quad (43)$$
$$e^{-j\frac{2\pi\Delta f}{c}D_{bs}+j\frac{2\pi f_c}{c}[(p-\tilde{p})d_T\cos(\mu_{Rbs}+\theta_T)-(q-\tilde{q})d_R\cos(\mu_{Rbs}-\theta_R)]}$$
$$e^{j\frac{2\pi f_c}{c}[v_T\Delta t\cos(\mu_{Rbs}+\gamma_T)-v_R\Delta t\cos(\mu_{Rbs}-\gamma_R)]}$$
$$e^{-\frac{\sigma^2_{Rbs}}{2}[\frac{2\pi\Delta f}{c}\frac{h_R+h_T-2h}{\sin\mu_{Rbs}\tan\mu_{Rbs}}+\frac{2\pi f_c}{c}(q-\tilde{q})d_R\sin(\mu_{Rbs}-\theta_R)]}$$
$$e^{-\frac{\sigma^2_{Rbs}}{2}[-\frac{2\pi f_c}{c}(p-\tilde{p})d_T\sin(\mu_{Rbs}+\theta_T)+\frac{2\pi f_c}{c}v_R\Delta t\sin(\mu_{Rbs}-\gamma_R)]}$$
$$e^{-\frac{\sigma^2_{Rbs}}{2}[\Delta t\zeta^2_{\Delta Z_{bs}}[\frac{2\pi}{\lambda}]^2\sin\mu_{Rbs}\cos\mu_{Rbs}]^2-\frac{2\pi f_c}{c}v_T\Delta t\sin(\mu_{Rbs}+\gamma_T)},$$
$$R^{DA}_{pq,\tilde{p}\tilde{q}}(\Delta t,\Delta f) = \frac{\eta_S}{2S}\sum_{s=1}^{S}\sum_{b=s-1}^{s}e^{-\frac{\Delta t\zeta^2_{\Delta Z_{sb}}}{2}[\frac{2\pi f_c}{c}\sin\mu_{Rsb}]^2} \quad (44)$$
$$e^{-j\frac{2\pi\Delta f}{c}D_{sb}+j\frac{2\pi f_c}{c}[(q-\tilde{q})d_R\cos(\mu_{Rsb}-\theta_R)-(p-\tilde{p})d_T\cos(\mu_{Rsb}+\theta_T)]}$$
$$e^{j\frac{2\pi f_c}{c}[v_T\Delta t\cos(\mu_{Rsb}+\gamma_T)-v_R\Delta t\cos(\mu_{Rsb}-\gamma_R)]}$$
$$e^{-\frac{\sigma^2_{Rsb}}{2}[\frac{2\pi\Delta f}{c}\frac{h_R+h_T}{\sin\mu_{Rsb}\tan\mu_{Rsb}}+\frac{2\pi f_c}{c}(q-\tilde{q})d_R\sin(\mu_{Rsb}-\theta_R)]}$$
$$e^{-\frac{\sigma^2_{Rsb}}{2}[-\frac{2\pi f_c}{c}(p-\tilde{p})d_T\sin(\mu_{Rsb}+\theta_T)+\frac{2\pi f_c}{c}v_R\Delta t\sin(\mu_{Rsb}-\gamma_R)]}$$
$$e^{-\frac{\sigma^2_{Rsb}}{2}[\Delta t\zeta^2_{\Delta Z_{sb}}[\frac{2\pi}{\lambda}]^2\sin\mu_{Rsb}\cos\mu_{Rsb}]^2-\frac{2\pi f_c}{c}v_T\Delta t\sin(\mu_{Rsb}+\gamma_T)}.$$

IV. Comparison with Measured Data

In this section, we compare the theoretical results in Section III with the AUVFest07 measured data in [8], collected at rough sea. Furthermore, we compare the derived spatial correlation function with the spatial correlation functions of the exponential model in [9], the particle-velocity model in [7], and the measured data in [9]. The close agreement between the analytical and measured statistics is observed.

The channel measurements in [8] are collected at $f_c = 17$ kHz and the speed of sound was $c = 1470$ m/s. The distance between the $\mathrm{T_x}$ and $\mathrm{R_x}$ was $R = 5$ km. The water, $\mathrm{T_x}$, and $\mathrm{R_x}$ depths were $h = 20$ m, $h_T = 19$ m, and $h_R = 18$ m, respectively. The $\mathrm{T_x}$ and $\mathrm{R_x}$ are equipped with vertically oriented transducer elements (i.e., $\theta_T = \theta_R = 90^\circ$). It is assumed that the $\mathrm{T_x}$ and $\mathrm{R_x}$ are relatively stationary, i.e., slightly moving with waves (i.e., $\gamma_T = \gamma_R = 90^\circ$).

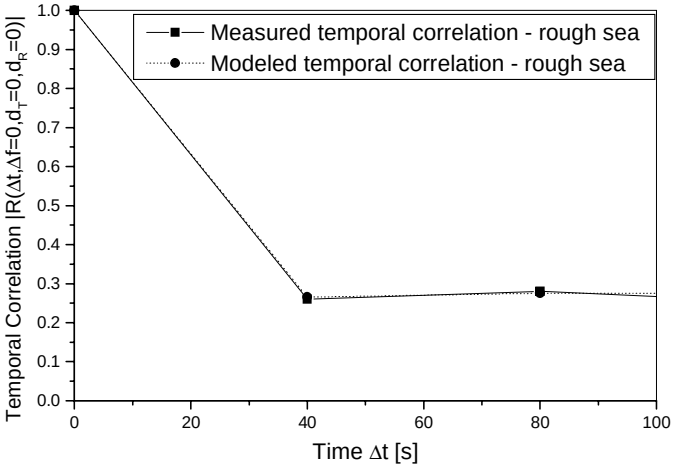

Fig. 3. The magnitude of the theoretical and measured temporal correlation functions for rough sea.

Fig. 3 compares the analytical temporal correlation function in (32) with the measured temporal correlation function in [8] for the rough sea environment. The analytical curve is obtained with the estimated parameters $K = 0.38$, $S = 1$, $B = 1$, $v_T = 0.005$ m/s, $v_R = 0.002$ m/s, $\zeta_{\Delta Z_{s=1,b=0}} = \zeta_{\Delta Z_{s=1,b=1}} = 0.0014$, $\zeta_{\Delta Z_{b=1,s=0}} = \zeta_{\Delta Z_{b=1,s=1}} = 0.006$, $\mu_{s=1,b=0} = 168^\circ$, $\mu_{s=1,b=1} = 171^\circ$, $\mu_{b=1,s=0} = 205^\circ$, $\mu_{b=1,s=1} = 210^\circ$, $\sigma_{s=1,b=0} = 2.55^\circ$, $\sigma_{s=1,b=1} = 3.1^\circ$, $\sigma_{b=1,s=0} = 10^\circ$, $\sigma_{b=1,s=1} = 12^\circ$, $\eta_S = 0.2$, and $\eta_B = 1-\eta_S$. The parameters S and B are visually estimated from Fig. 2d in [8]. The rest of the parameters are estimated using the maximum likelihood

method described in [12]. The parameters R, h, h_T, h_R, γ_T, γ_R, θ_T, θ_R, and $\alpha_{Rdpp} \approx \pi$, are selected to match the measurement conditions as described above. Fig. 4 compares

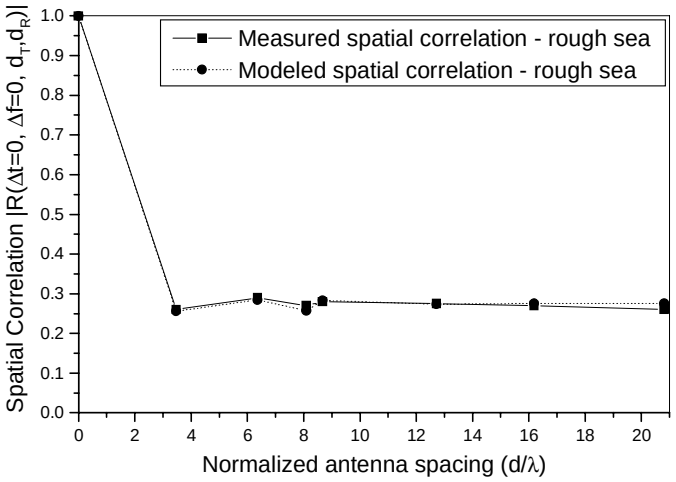

Fig. 4. The magnitude of the theoretical and measured spatial correlation functions for rough sea.

the analytical spatial correlation function in (32) with the measured spatial correlation function in [8] for the rough sea environment.The analytical curve in Fig. 4 is obtained using the same parameters as in Fig. 3. Finally, Fig. 5 compares the spatial correlation in (32) with the analytical spatial correlation in [7] and the analytical and empirical spatial correlations in [9]. The ASCOT01 channel measurements are collected at

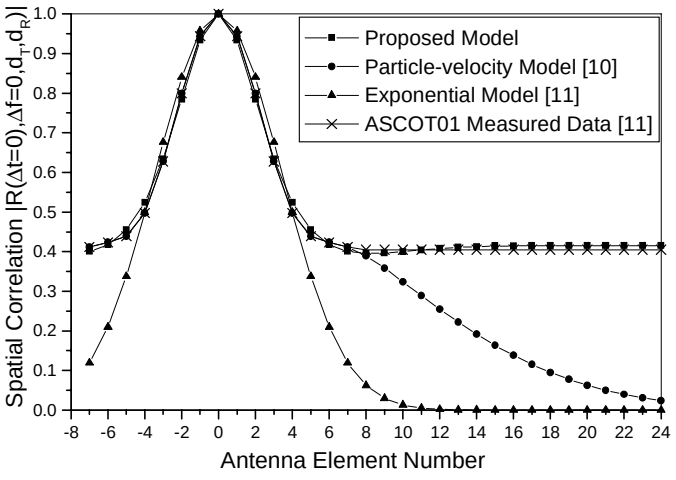

Fig. 5. Comparison of the analytical spatial correlations in (32), [7], and [9] with the empirical spatial correlation in [9].

the carrier frequency 1.2 kHz and the speed of sound was $c = 1440$ m/s (i.e., λ=1.2 m) [9]. The distance between the $\mathrm{T_x}$ and $\mathrm{R_x}$ was $R = 10$ km. The water, $\mathrm{T_x}$, and $\mathrm{R_x}$ depths were $h = 103$ m, $h_T = 50$ m, and $h_R = 50$ m, respectively. The $\mathrm{R_x}$ was equipped with 33 vertically oriented transducer elements (i.e., $\theta_R = 90^\circ$) with $L = d_R = 0.5$ m element spacing, while the $\mathrm{R_x}$ was equipped with one vertical transducer (i.e., $\theta_T = 90^\circ$). The vertical correlation is calculated with respect to eighth element from the bottom of the 33-element array. The analytical spatial correlation in (32) is obtained with the estimated parameters $K = 0.71$, $S = B = 1$, $\mu_{s=1,b=0} = 173.8^\circ$, $\mu_{s=1,b=1} = 173.4^\circ$, $\mu_{b=1,s=0} = 183^\circ$, $\mu_{b=1,s=1} = 184.5^\circ$, $\sigma_{s=1,b=0} = 9.1^\circ$, $\sigma_{s=1,b=1} = 10.2^\circ$, $\sigma_{b=1,s=0} = 5.59^\circ$, $\sigma_{b=1,s=1} = 8.89^\circ$, $\eta_S = 0.44$, and $\eta_B = 1 - \eta_S$. The parameters R, h, h_T, h_R, θ_T, θ_R, and $\alpha_{Rdpp} \approx \pi$, are selected to match the measurement conditions described above. For the reference, Fig. 5 also shows the spatial correlation functions of the exponential model in [9], i.e, $\exp\{-L^2/(2\lambda)^2\}$ and the particle-velocity model in [7] (with parameters $\Lambda_b = 0.56$, $\mu_b = 183^\circ$, $\mu_s = 173^\circ$, $\sigma_b = 2.29^\circ$, and $\sigma_s = 8^\circ$). One can observe that the proposed model provides a closer match with the experimental correlation than the models in [7] and [9].

The close agreement between the analytical and measured statistics in Figs. 3-5 confirms the utility of the proposed model.

V. Conclusions

This paper proposed the geometry-based statistical model for MIMO SWA fading channels. From the statistical model, the corresponding space-time-frequency correlation function is derived. Finally, the derived statistics are compared with the empirically obtained channel statistics and the close agreement is observed.

References

[1] M. Stojanovic, "Recent advances in high-speed underwater acoustic communications," *IEEE J. of Oceanic Eng.*, vol. 21, pp. 125–136, Apr. 1996.

[2] M. Badiey, Y. Mu, J. A. Simmen, and S. E. Forsythe, "Signal variability in shallow-water sound channels," *IEEE J. of Oceanic Eng.*, vol. 25, pp. 492–500, Oct. 2000.

[3] D. B. Kilfoyle and A. B. Baggeroer, "The state of the art in underwater acoustic telemetry," *IEEE J. of Oceanic Eng.*, vol. 25, pp. 4–27, Jan. 2000.

[4] A. Zielinski, Y-H. Yoon, and L. Wu, "Performance analysis of digital acoustic communication in a shallow water channel," *IEEE J. of Oceanic Eng.*, vol. 20, pp. 293–299, Oct. 1995.

[5] C. Bjerrum-Niese, L. Bjorno, M. A. Pinto, and B. Quellec, "A simulation tool for high data-rate acoustic communication in a shallow-water, time-varying channel," *IEEE J. of Oceanic Eng.*, vol. 21, pp. 143–149, Apr. 1996.

[6] M. Chitre, "A high-frequency warm shallow water acoustic communications channel model and measurements," *J. Acoust. Soc. Am.*, vol. 122, pp. 2580–2586, Nov. 2007.

[7] A. Abdi and H. Guo, "Signal correlation modeling in acoustic vector sensor arrays," *IEEE Trans. on Signal Processing*, vol. 57, pp. 892–903, Mar. 2009.

[8] T. C. Yang, "An experimental study of the environmental impact on the performance of high-frequency phase-coherent underwater acoustic communications," submitted for publication.

[9] T. C. Yang, "A study of spatial processing gain in underwater acoustic communications," *IEEE J. of Oceanic Eng.*, vol. 32, pp. 689–709, July 2007.

[10] L. M. Brekhovskikh and Y. Lysanov, *Fundamentals of ocean acoustics 2e*. Springer, Berlin, 1991.

[11] I. S. Gradshteyn and I. M. Ryzhik, *Table of Integrals, Series, and Products* . San Diego, CA: A. Jeffrey, Academic, 5th ed., 1994.

[12] A. G. Zajić, G. L. Stüber, T. G. Pratt, and S. Nguyen, "Wideband mimo mobile-to-mobile channels: geometry-based statistical modeling with experimental verification," *IEEE Trans. on Veh. Tech.*, vol. 58, pp. 517-534, Feb. 2009.